narra j

Original Article

HUVECs-derived exosomes increase neovascularization and decrease limb necrosis in hindlimb ischemia

Muhamad T. Ismail[1*], Dyah W. Anggrahini[1], Sofia M. Haryana[2] and Budi Y. Setianto[1]

[1]Department of Cardiology and Vascular Medicine, Faculty of Medicine, Public Health and Nursing, Universitas Gadjah Mada, Yogyakarta, Indonesia; [2]Department of Cell Histology and Biology Faculty of Medicine, Public Health and Nursing, Universitas Gadjah Mada, Yogyakarta, Indonesia

*Corresponding author: mutaufiq_is@yahoo.com

Abstract

Chronic limb-threatening ischemia (CLTI) is the most severe manifestation of peripheral arterial disease (PAD) and imposes a significantly high burden due to its high risk of mortality and amputation. Revascularization is the first-line treatment for CLTI; however, the amputation rate remains high, and approximately one-third of patients are not eligible for this treatment. Therefore, there is an urgent need for more effective therapeutic strategies. The aim of this study was to investigate the effects and mechanisms of human umbilical vein endothelial cells (HUVECs)-derived exosomes on neovascularization and the degree of necrosis in a hindlimb ischemia model and to study the biological processes underlying their mechanisms. This is an in vivo experimental study with a post-test-only control group design. Forty BALB/c mice were randomized to receive injections of exosomes, conditioned media, and phosphate-buffered saline (PBS) one day after unilateral double ligation. A sham-operated group was also included as a control. Capillary density, arteriole lumen diameter, and histopathological necrosis were measured after seven days, while clinical necrosis was observed daily. MicroRNA profiling, in silico analysis, and transcriptomic analysis of vascular endothelial growth factor (VEGF) mRNA expression were performed to determine the possible biological processes. No amputation was found in the exosome group, as well as in the conditioned media and sham-operated groups, compared to three out of seven mice (43%) in the PBS group. The capillary density was higher in the exosome than in the PBS group (p=0.026). The arteriole lumen diameter in the exosome group was larger than in the PBS (p=0.033) and sham-operated (p=0.034) groups. The scores of clinical necrosis and histopathological necrosis in the exosome group were lower than the PBS group (p=0.005), while the histopathological necrosis scores were also lower but statistically insignificant. In silico analysis showed improvement in neovascularization and necrosis, possibly through energy regulation, PI3K/AKT and TGF-β activation, the ubiquitin-proteasome system, and tyrosine kinases receptors. HUVEC exosomes were associated with lower VEGF mRNA expression, which may indicate a more effective compensatory mechanism under ischemic conditions. The exosome group had the lowest VEGF mRNA expression compared to other groups, although the difference was not statistically significant. This study highlights that HUVECs-derived exosomes improve neovascularization and decrease necrosis in a hindlimb ischemia mice model, potentially by modulating several possible mechanisms.

Keywords: Exosome, neovascularization, amputation, hindlimb ischemia, chronic limb-threatening ischemia

Introduction

Peripheral arterial disease (PAD) is a chronic vascular condition resulting from atherosclerosis, affecting an estimated 3.7% to 10% of the global population [1-3]. One of the most severe

https://narraj.org/

Received: August 22, 2024 - Accepted: November 20, 2024- Published online: November 22, 2024

manifestations of PAD is chronic limb-threatening ischemia (CLTI), a growing global health concern that incurs substantial healthcare costs [4]. Standard conservative therapies for CLTI are often inadequate, with a 27% rate of limb amputation and an 18% mortality rate within the first year following diagnosis [5]. While revascularization remains the primary intervention, many patients remain at high risk of amputation and death, especially those who are not candidates for surgery due to anatomical or physiological limitations [6-9]. Approximately one-third of patients are not eligible for revascularization [10]. These challenges underscore the urgent need for alternative therapeutic approaches.

Several clinical trials involving peripheral blood mononuclear cells (PBMNCs) and bone marrow mononuclear cells (BMMNCs) have been conducted for CLTI treatment [8,11,12]. Unfortunately, these cell-based therapies have not shown significant improvements in key outcomes such as amputation rates or wound healing [8,11,12]. This is likely due to issues such as high immunogenicity and poor cell survival in ischemic environments [13,14]. Emerging regenerative therapies, particularly those based on genetic and cell-based technologies, are showing promise. Among these, microRNAs (miRNAs) have attracted attention for their role in promoting neovascularization [8,15]. However, the clinical use of 'naked' miRNAs has been hampered by stability issues [16].

Exosomes, small extracellular vesicles containing lipids, miRNAs, and proteins, offer a promising alternative due to their ability to facilitate intercellular communication. Exosomes offer greater stability and enhanced therapeutic potential compared to free miRNAs [16]. Importantly, exosomes exhibit lower immunogenicity and reduced tumorigenic potential compared to other cell-based therapies [17,18]. Exosomes derived from human CD34+ stem cells have shown promising effects on angiogenesis in preclinical models of hindlimb ischemia [19].

Human umbilical cord mesenchymal stem cells (hucMSCs) possess several advantages over other stem cell sources, including ease of extraction, low cost, non-invasive collection methods, and favorable ethical considerations. Furthermore, hucMSCs have a high proliferation capacity and low immunogenicity, reducing the risk of rejection or adverse immune responses [17,20]. Human umbilical vein endothelial cells (HUVECs), derived from hucMSCs, demonstrate robust angiogenic potential, suggesting that exosomes derived from these cells may offer therapeutic benefits for CLTI [21]. Despite these advances, there has been limited exploration of exosomes derived from hucMSCs for CLTI treatment.

HUVEC-derived exosomes have been shown to improve cardiac function and reduce fibrosis in models of myocardial infarction; however, their potential to promote arteriogenesis and angiogenesis in peripheral ischemic conditions remains unexplored [22]. The aim of this study was to investigate the effects of HUVECs-derived exosomes on neovascularization and necrosis in the hindlimb ischemia (HLI) model and to explore the underlying biological processes through miRNA profiling.

Methods

Study design and setting

This in vivo experimental study with a post-test-only control group design was conducted at the Faculty of Medicine, Public Health, and Nursing, Universitas Gadjah Mada, Yogyakarta, Indonesia, between May 2022 and February 2023. This study utilized an animal model to assess the effects of exosomes derived from HUVECs on PAD. Experimentation was conducted on 24-week-old BALB/c mice. The mice were divided into four treatment groups: sham-operated group, HLI + exosome group, HLI + conditioned media group, and HLI + phosphate-buffered saline (PBS) group. Assessment of neovascularization (capillary density and diameter of arterioles) and histopathological necrosis within ischemic limbs was performed on day seven post-intervention. Clinical necrosis was assessed daily. MicroRNA profiling, in silico analysis, and transcriptomic analysis of vascular endothelial growth factor (VEGF) mRNA expression were performed to determine the possible biological processes.

Eligibility criteria for HUVECs sample collection

The inclusion criteria of HUVECs involved obtaining umbilical cords from healthy mothers who had a full-term pregnancy of 37–40 weeks and delivered by cesarean section or vaginal delivery.

To assure the quality of the endothelial cells, mothers without any known chronic diseases, including diabetes, hypertension or cardiovascular diseases, were selected. All parents provided their informed consent before collecting the umbilical cord blood. Pregnant women with preeclampsia, gestational diabetes, or intrauterine infections were excluded since these conditions could affect the quality and regenerative capacity of the HUVECs. Furthermore, umbilical cords from preterm births (before 37 weeks of gestation) or deliveries with placental inadequacy were also excluded, as these could modify the endothelial cell composition. Any umbilical cords that were noticed to be infected or damaged were also excluded in order to keep the collected HUVEC samples intact.

Cell culture and exosome isolation

After obtaining the parents' consent, HUVECs were isolated from the proximal portion of the infant's umbilical cord. This process did not negatively affect the infant or the parents, as it involved collecting tissue from a part of the umbilical cord that would otherwise be discarded. Following the proximal cut, the umbilicus was cleared of blood by venipuncture and delivered to the laboratory within 24 hours. A cannula was used to cleanse any remaining blood with a buffer solution, and the tissues were isolated using 0.2% collagenase for 15 minutes at 37°C. The endothelial and subendothelial layers were collected via centrifugation and washed three times with PBS. The cultures, containing 2 million HUVECs each, were placed on 100 mm diameter discs and incubated for three days. After cobblestone formation, the cells were sub-cultured using the warm trypsin method. The petri dish containing HUVECs was placed in a hypoxic chamber to create hypoxic conditions, which was called conditioned media. This conditioned media was used as one of the interventions in this study. The conditioned media was transferred into a sterile tube, followed by the addition of the Invitrogen Exosome Isolation Kit (Thermo Fisher Scientific, Waltham, USA). After overnight incubation at 2–8°C, the samples were centrifuged. The supernatant was removed, leaving the exosome-containing pellet, which was suspended in a 1:1 solution of PBS and 0.9% NaCl.

Exosome characterization and quantification

Exosome characterization was carried out using flow cytometry (BD FACSAria, New Jersey, USA) and the Exosome Isolation and Analysis Kit - Flow Cytometry, Plasma (CD63/CD81, Abcam, Waltham, USA, ab267479). Briefly, following overnight incubation, 5 µL of CD63 and CD81 antibodies, specific to exosomes, were added to the tube containing bead-bound exosomes and gently mixed. The mixture was incubated in the dark at 2–8°C for 60 mins. After incubation, the sample was washed with 1 mL of 1X Assay Buffer, and the beads were collected using a magnetic rack or centrifuged at 2,500×g for 5 mins. The beads were then resuspended in 350 µL of 1X Assay Buffer and analyzed using a flow cytometer. Positive beads were identified by a fluorescent peak in the FL2 channel.

Quantification and size distribution of exosomes were determined by Nanoparticle Tracking Analysis (NTA) using the ViewSizer 3000 (HORIBA Scientific, Irvine, USA). The NTA system was equipped with blue (445 nm), green (520 nm), and red (635 nm) lasers set at 400 mW, 18 mW, and 8 mW, respectively. Camera gain was set to 24 dB, the frame rate to 30 frames per second, and exposure time to 14 ms during video recording. The sample was automatically stirred for five seconds. Extracellular vesicle (EV) concentration data were presented as particles/mL. In brief, samples were diluted 17.5-fold with water for injection (WFI), resulting in a final size range of 20–1000 nm and a concentration of 3.4×10^8 particles per mL.

Animal sample size and eligibility

The Federer's formula calculated the minimum sample size required as six subjects per group. The size was increased to seven animals per group to compensate for a possible 10% dropout. Furthermore, three additional mice were added for miRNA and mRNA analysis, making the total number of mice per group to be ten. With four groups in the study, the total sample size was 40 mice. Eligible subjects were 24-week-old healthy BALB/c male mice weighing 29–45 g, obtained from the Animal Model Care Unit, Universitas Gadjah Mada, Yogyakarta, Indonesia. Animals with any signs of health problems during the acclimatization period or the study process were

excluded. Animals with a weight reduction of 10%, a vein rupture or a femoral nerve injury after ligation, or those who suffered from any conditions resulting in death were dropped out.

Acclimatization and randomization

The mice were raised in the Animal Laboratory of the Department of Pharmacology and Therapy, Faculty of Medicine, Public Health, and Nursing, Universitas Gadjah Mada, Yogyakarta, Indonesia. They were housed under 12 hours of natural light-dark cycle, with humidity at 50–70%, and had free access to standard food and water. Mice were adapted for seven days prior to intervention and went through routine health monitoring. The mice were randomly allocated into four study groups, ten animals for each group. Twenty-eight mice were used for analyzing capillary density, arteriole area, and necrotic stage (n=7); twelve mice were used for profiling miRNA analysis (n=3).

Study groups and interventions

In this study, there were four groups: HLI + exosome group (n=10), HLI + conditioned media group (n=10), HLI + PBS group (n=10), and sham-operated group (n=10). Detailed visualization of study groups and experimental procedure for each group is presented in **Figure 1**. HLI model was generated after seven days of adaptation by ligating both the right iliac and femoral artery using 7.0 silk. The left limb was not given intervention and served as an internal control. Before ligation, the mice were anesthetized with ketamine (80 mg/kg), xylazine (12.5 mg/kg), and acepromazine (3 mg/kg) via intraperitoneal injection. After 24 hours, the mice were assigned to receive intramuscular injections of exosome, conditioned media or PBS. In the exosome group, 25 µL of isolated exosomes were diluted 40× with sterile PBS to reach 1 ml and injected into four sites (two in adductor and two gastrocnemius muscles) in each animal; 25 µL exosomes equal to 850.000 particles/mouse. In the conditioned media group, 25 µL of conditioned media was also diluted 40× with sterile PBS to reach 1 ml and injected in the four same sites. A total of 1 mL of PBS was also injected in the same places in the PBS group. The sham-operated group underwent the same surgical procedure except for ligation. All mice were sacrificed seven days after the intervention.

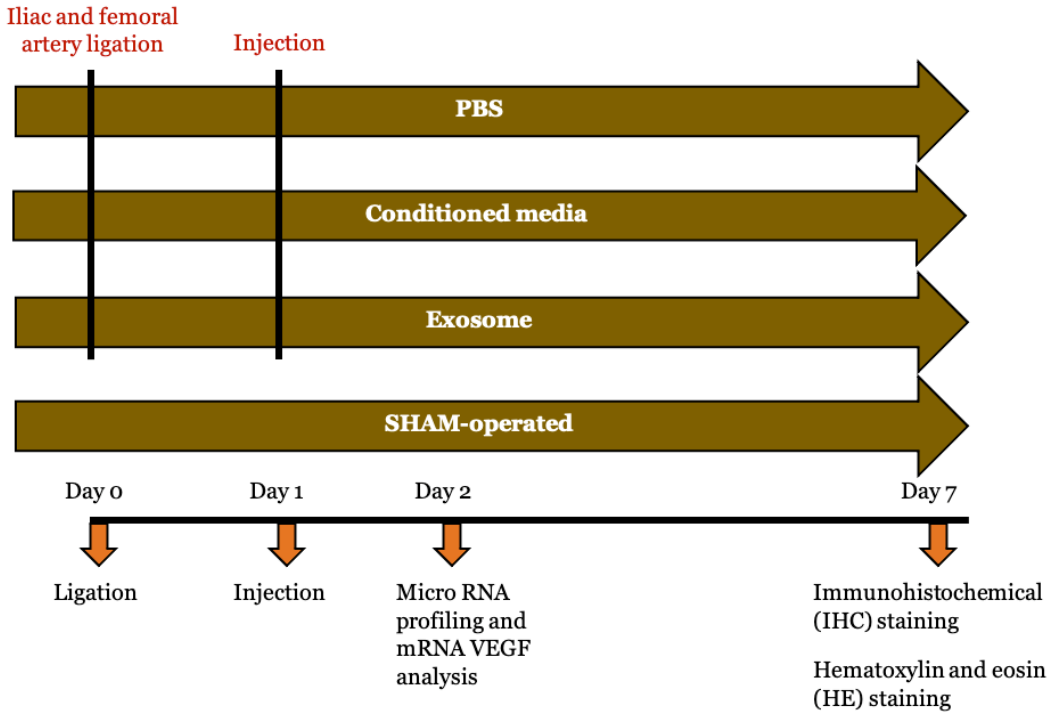

Figure 1. Study groups and experimental protocol for each group.

Macroscopic assessment of necrotic degree

On the seventh day after the intervention, the ligated limbs of 28 mice were evaluated clinically using Wang grading system [23] by an independent anatomist in a blinded manner. According to this grading system, the degree of necrosis was categorized into five grades: grade 0 indicates a normal hindlimb without necrosis; grade I represents mild discoloration; grade II indicates moderate discoloration; grade III signifies severe discoloration or subcutaneous tissue loss or necrosis; and grade IV corresponds to any amputation of the hindlimb [23].

Immunohistochemical (IHC) staining

The gastrocnemius and adductor muscles were collected in sections of approximately 50–100 mg, then embedded in paraffin blocks and sectioned at 4 µm. The slides were deparaffinized and rehydrated using a series of xylene and alcohol solutions. Antigen retrieval was performed using a heating method with citrate buffer, followed by blocking endogenous peroxidase activity with 3% H_2O_2. To minimize nonspecific binding, the slides were incubated in 1% BSA in PBS. The gastrocnemius and adductor muscle slides were then incubated with primary antibodies: anti-CD31 (1:100, ABclonal, Woburn, USA, A0378) and α-SMA (1:200, ABclonal, Woburn, USA, A1011) as first antibodies. The use of these markers was based on their roles as markers for neovascularization [24]. A goat anti-rabbit horseradish peroxidase (HRP) label was applied as the secondary antibody, followed by staining with diaminobenzidine tetrahydrochloride (DAB). Angiogenesis was assessed by counting the ratio of total CD31-positive cells in the gastrocnemius muscle of the right limb (with ligation as HLI model) compared to the left limb (without ligation) across 10 fields of view for each sample at 400× magnification, using ImageJ software (Olympus CX33, Tokyo, Japan). The left limb serves as internal control, as stated in a previous study [19]. Arteriogenesis in each mouse was evaluated by calculating the ratio of mean total arteriole lumen area in the right adductor muscle samples compared to the left adductor muscle samples, also using ImageJ software at 400× magnification. The ratios of mean total arteriole lumen area from all mice in each group were calculated and summed to determine the overall mean ratio for each group. This final mean value was then used for analysis.

Hematoxylin and eosin (H&E) staining

The gastrocnemius muscles from the right hindlimb were collected in sections of approximately 50–100 mg, then embedded in a paraffin block and sectioned into 4 µm slices. The slides were deparaffinized and rehydrated using a series of xylene and alcohol solutions. Subsequently, the slides were stained with Mayer's hematoxylin for 3 mins and 0.5% eosin for 1 min. Pathological changes in the gastrocnemius muscle were then observed under a light microscope at 400× magnification (Olympus CX33, Tokyo, Japan). Histopathological assessment of the degree of necrosis was conducted on the gastrocnemius muscle preparations, utilizing the Carter grading system for mice [25], as detailed in **Table 1**.

Table 1. Histopathology of necrosis scoring system used in this study

Numerical score	Skeletal muscle histopathology
0	No abnormal findings
1	Mild localized mononuclear cell infiltration
2	Mild multifocal mononuclear cell infiltration, rare necrotic fibers
3	Moderate generalized mononuclear cell infiltration, occasional necrotic fibers
4	Moderate cell infiltration including polymorphonuclear cells (PMN), mild multifocal necrosis
5	Marked cell infiltration including PMN, moderate multifocal fiber necrosis
6	Marked cell infiltration including PMN, moderate generalized fiber necrosis
7	Severe cell infiltration including PMN, marked multifocal fiber necrosis
8	Severe cell infiltration, hemorrhage possible with severe fiber necrosis
9	Massive cell infiltration, hemorrhage possible with severe generalized fiber necrosis
10	Massive cell infiltration, and complete loss of tissue architecture

Isolation and miRNA profiling

The total RNA of the sample was extracted using the Quick-RNA FFPE Kit (Zymo Research, Irvine, USA) following the manufacturer's instructions. The purity of the RNA was initially assessed with the ND-Nanodrop1000 spectrometer (Thermo Scientific, Wilmington, USA), and

the quantification of RNA was measured with Qubit RNA HS Assay Kits (Thermo Fisher Scientific, Waltham, USA). Furthermore, the quality and integrity of the RNA were evaluated using the TapeStation (Agilent Technologies, Palo Alto, USA).

Subsequently, the NanoString nCounter system assay was conducted using the NanoString platform and the nCounter mouse v.15 miRNA Assay CSO (which includes one panel for 12 assays) (NanoString Technologies, Seattle, USA), in accordance with the manufacturer's guidelines. This panel analyzes up to 577 miRNAs, in addition to 33 murine-associated viral miRNAs, four mRNA probes, and 23 internal reference controls. miRNA profiling was carried out for each group, starting with 3 µL of isolated RNA (approximately 150 ng). The samples were processed using the automated nCounter Prep Station (NanoString Technologies, Seattle, USA); following hybridization, they were purified and immobilized on a sample cartridge for quantification and data collection using the nCounter Digital Analyzer (NanoString Technologies, Seattle, USA).

Transcriptomic analysis of vascular endothelial growth factor (VEGF) mRNA expression

For the transcriptomic analysis of VEGF mRNA expression, adductor muscle tissues (50–100 mg) were collected from mice euthanized on day 2 and preserved in RNA Later (Favorgen Biotech Corporation, Taipei, Taiwan) at -20°C. The preserved tissue was then transferred to a new tube containing RNAiso Plus (Trizol) (Thermo Fisher Scientific, Waltham, USA) and homogenized. An additional 0.5 cc of RNAiso Plus reagent was added, followed by 0.2 cc of chloroform. The mixture was vortexed and incubated at room temperature for 2–3 minutes. After centrifugation at 15,000 revolutions per minute (RPM) for 15 mins at 4°C, the aqueous phase was collected and mixed with an equal volume of isopropanol (1:1). This mixture was centrifuged again at 15,000 RPM for 10 mins, after which the RNA pellet was washed with 70% ethanol, resuspended in 30–50 µL of RNase-free water, and incubated at 55°C for 10 mins. The RNA was subsequently stored at -80°C.

To synthesize complementary DNA (cDNA), 2000 ng of RNA was mixed with 1 µL of Oligo DT and DEPC-treated (SMOBio, Hsinchu, Taiwan) water to achieve a final volume of 10 µL. This mixture was incubated at 70°C for 5 mins and then placed on ice. For cDNA synthesis, a reaction mixture comprising 4 µL of 5× RT-Buffer, 5 µL of DEPC-treated water, and 1 µL of RTase/RI Enzyme Mix (SMOBio, Hsinchu, Taiwan) was added to the RNA mixture. The reaction was incubated in a polymerase chain reaction (PCR) machine at 25°C for 10 mins, 42°C for 50 mins, and 85°C for 5 mins, after which the cDNA was stored at -20°C.

Real-time PCR was conducted to measure VEGF mRNA levels, using glyceraldehyde 3-phosphate dehydrogenase (GAPDH) gene as a housekeeping gene. The primer sequences used were: VEGF forward ACCTCCACCATGCCAAGT, reverse TTGGTCTGCATTCACATCTG; GAPDH forward TCTCGCTCCTGGAAGATGGTGA, reverse GGCACAGTCAAGGCTGAGAATG. The PCR conditions included initial denaturation at 94°C for 2 minutes, followed by 40 cycles of denaturation at 94°C for 10 seconds, annealing at 64°C for 1 min, and extension at 72°C for 1 min, with a final elongation step at 72°C for 10 mins. GAPDH PCR was performed under similar conditions but with an annealing temperature of 60°C. PCR products were analyzed by electrophoresis on a 2% agarose gel from Agarose S (Nippon Gene, Tokyo, Japan), and VEGF mRNA expression was quantified by calculating the VEGF/GAPDH ratio using the ImageJ software program (National Institutes of Health, Bethesda, USA).

The assessment of VEGF mRNA expression was performed by comparing cycle threshold (CT) values. The CT value for VEGF gene was normalized against the CT value of GAPDH to obtain the delta CT value. Subsequently, the delta CT values for the exosome, conditioned media, and PBS groups were compared to the average delta CT value of the sham-operated group, serving as a control. Results were expressed as fold changes relative to the sham-operated group.

In silico analysis of differential miRNA expression and pathway involvement

In silico analysis was conducted to evaluate changes in miRNA expression following the administration of exosomes, conditioned media, PBS, and sham-operated treatment. Total RNA was isolated from adductors, and a NanoString analysis was conducted using nSolver Analysis Software (V4.0) (NanoString Technologies, Seattle, USA), with fold changes (FC) represented on a log2 scale. A significance level of $|FC| \geq 1.5$ and $p<0.05$ was employed as the cut-off threshold

for selecting statistically significant miRNAs. Pathway and Gene Ontology analyses were used to evaluate the functional enrichment of these miRNAs using multiMiR R library (Bioconductor, Seattle, USA), which integrates multiple databases, including miRecords, MIRTarbase, miRDB, TargetScan, and miRanda. For the purpose of pathway and Gene Ontology biological process analyses Metascape (http://metascape.org) was employed. Further analysis of the miRNAs pathways was carried out using miRPath v4.0 (TarBase v8.0 database) (Diana Tools, Volos, Greece).

Statistical analysis

The data are expressed as either mean ± standard deviation (SD) or median with minimum to maximum values. All samples were evaluated for normality of data using Shapiro-Wilk test since the sample size was below 50. Next, Levene's test was carried out to assess the homogeneity of the data. The differences in the mean total arteriole lumen area ratio among groups were tested by one-way ANOVA because the data were normally distributed and homogeneous, while the mean capillary density, predicted by mean CD31 levels, was analyzed using Kruskal-Wallis test since the data distribution from PBS group was not normal. The one-way ANOVA revealed significant differences in the mean total arteriole lumen area ratio; thereby, a post-hoc test using Tukey test was performed to confirm these differences. The Kruskal Wallis test used for mean CD31 levels indicating capillary density showed significant results. Hence, further analysis was carried out using the Mann-Whitney U test and independent sample Student t-test to compare between two groups.

The differentially expressed miRNAs were identified using the Student t-test, with those showing a ≥1.5-fold change, and an adjusted $p<0.05$ considered statistically significant. Adjustment of p-value was executed using the Benjamini Hochberg method to prevent a false discovery rate due to multiple tests done from numerous expressed miRNAs. Functional analysis was conducted through Gene Ontology analysis to clarify the associated biological functions. Pathway and Gene Ontology analyses were carried out using Metascape, and the results were ranked according to enrichment scores to highlight the most relevant functions and pathways. Statistical analysis was performed using SPSS 22 software for Windows (IBM, New York, USA).

Results

From a total of 40 mice, one from the conditioned media group died during the period of study. Therefore, the remaining mice were used to assess mean total arteriole lumen area ratio, capillary density, and degree of necrosis; conditioned media (n=6), exosome (n=7), PBS (n=7) and sham-operated group (n=7). Another 12 mice underwent the miRNA analysis (n=3 per group).

Effect of HUVECs-derived exosomes on capillary density and arteriole area

The representative histopathological picture showing the angiogenesis (capillary density) from different study groups is presented in **Figure 2**. The ratio of CD31-positive cells in the ischemic to nonischemic limb showed that there were significant differences between the four groups ($p=0.026$). Further analysis showed that the CD31 ratio was significantly higher in the exosome group compared to the PBS group (1.28; 95%CI: 0.33–2.25 vs 0.25; 95%CI: 0.00–0.89; $p=0.026$) (**Figure 3**). The CD31-positive cell ratio in the exosome group was not significantly different compared to the conditioned media group (1.31±0.77 vs 0.56±0.45; $p=0.058$) and sham-operated group (1.31±0.77 vs 0.97±0.18; $p=0.263$) (**Figure 3**). Analysis of the PBS and sham-operated group showed a significant difference in CD31 ratio (0.25; 95%CI: 0.00–0.89 vs 0.96; 95%CI: 0.74–1.50; $p=0.011$) (**Figure 3**).

The mean total arteriole lumen area ratio, which indicates arteriogenesis, had significant differences among the four groups ($p=0.021$). The mean ratio of arteriole area in the exosome group was significantly higher than the PBS group (4.28±3.13 vs 1.32±1.08; $p=0.033$) and the sham-operated group (4.28±3.13 vs 1.23±0.50; $p=0.034$) and higher compared to the conditioned media group but statistically insignificant (4.28±3.13 vs 2.44±1.31; $p=0.310$) (**Figure 4** and **Figure 5**).

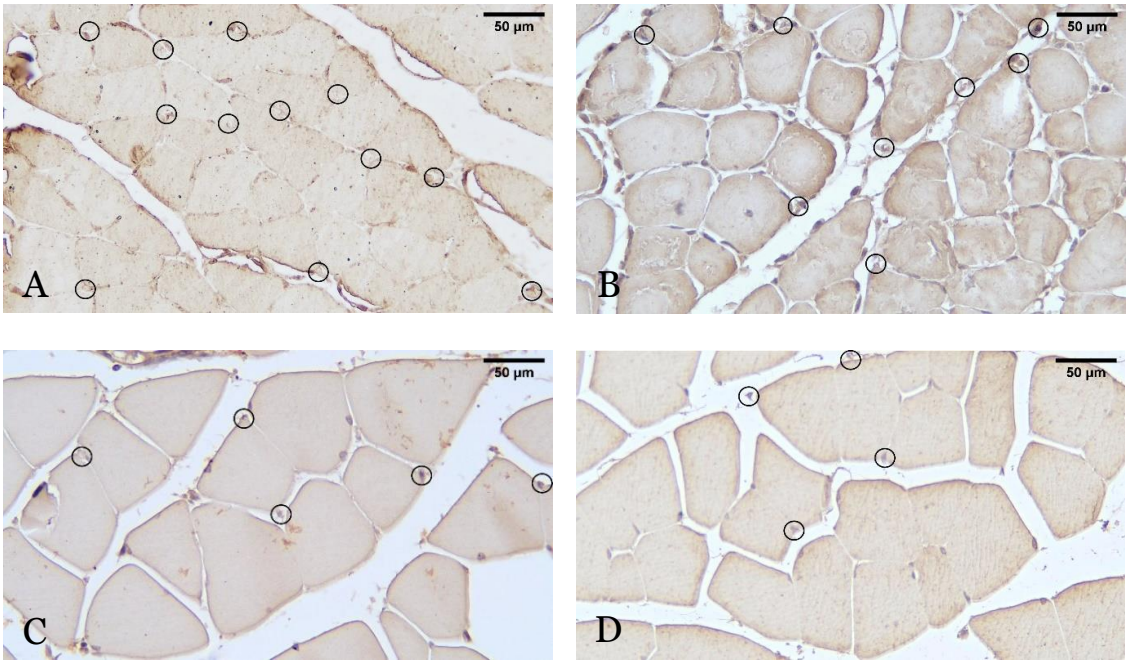

Figure 2. Histopathological representative picture showing the angiogenesis of adductor muscles from four different study groups using immunohistochemical (IHC) staining, with 400× magnification. Angiogenesis after hindlimb ischemia (HLI) and administration of exosomes (A), conditioned media (B) and PBS (C), and non-HLI sham-operated control (D) are assessed by measuring the numbers of CD31+ cells, which indicated by circles. The scale bar is equivalent to 50 µm.

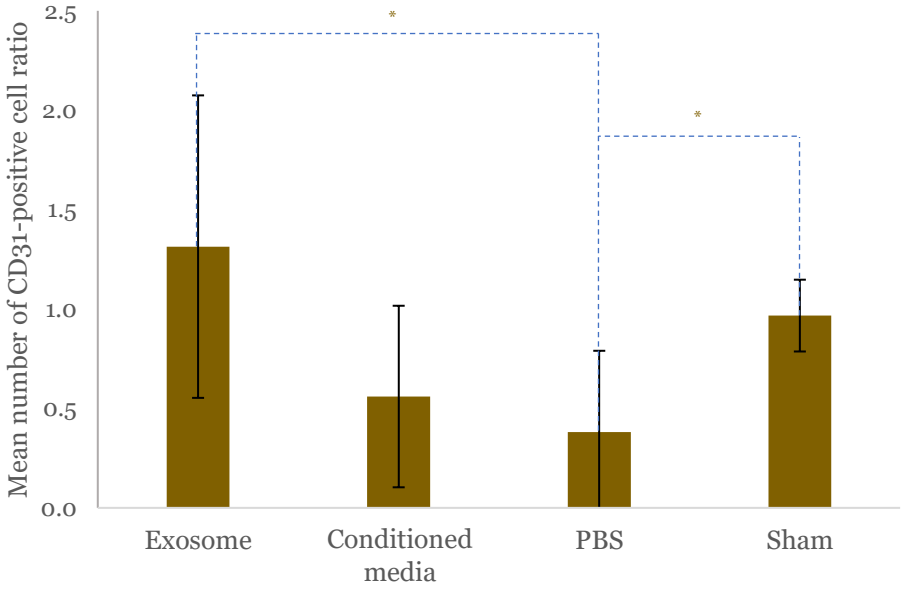

Figure 3. Comparison of mean CD31 positive cell ratio as a predictor of capillary density between exosome, conditioned media, PBS, and sham-operated groups. The ratio was calculated by comparing the total CD31-positive cells in the gastrocnemius muscle of the limb with ligation as hindlimb ischemia (HLI) model compared to contralateral limb without ligation. Black vertical lines depict standard deviation of mean from each group. The asterisk (*) indicates statistical significance.

Necrosis assessment after treatment of HUVECs-derived exosome

Clinical necrosis degree was assessed and classified into five grades based on the grading system by Wang, and the results are presented in **Figure 6** and **Figure 7**. The exosome group, on average, showed clinical necrosis of grade 1, characterized by black discoloration mainly on the nails and a darker red color on the ligated foot (**Figure 6**). The conditioned media group

exhibited clinical necrosis of grade 2, evidenced by black coloration on the nails and a clearer dark red color on the ligated foot compared to the control foot. In the PBS group, there were three mice that experienced autoamputation of the ligated foot: two mice on day 4 and one mouse on day 5, thus classified as grade 4. Meanwhile, in the sham-operated group, normal-looking feet with white nails and consistent foot coloration between ligated and control feet were observed, consistent with grade 0 appearance.

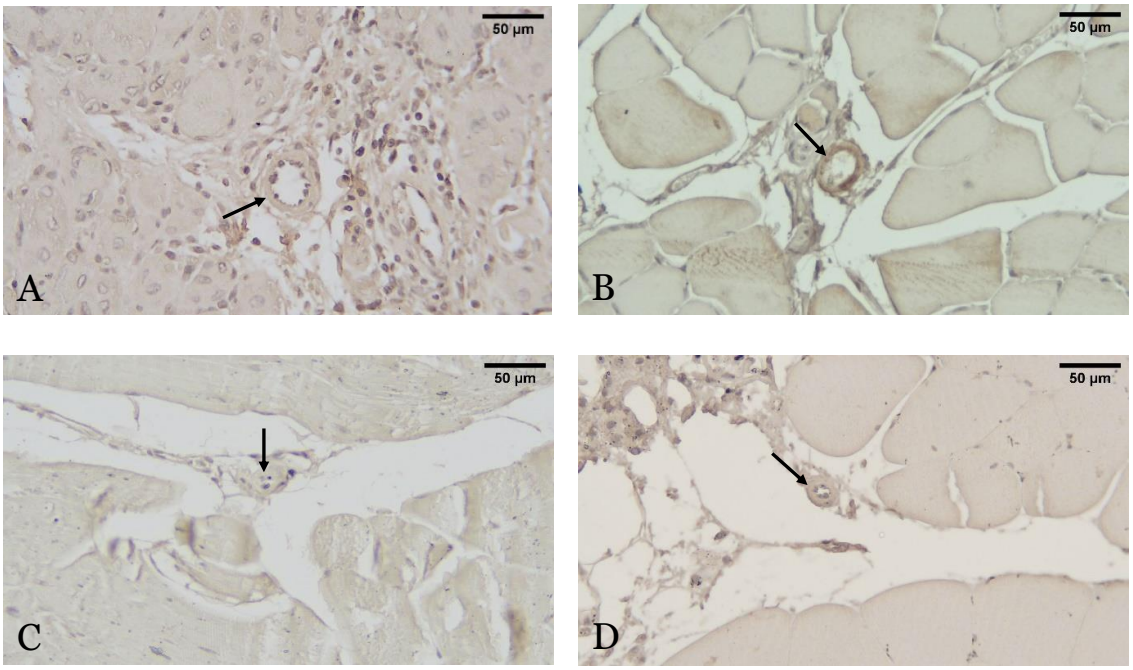

Figure 4. Histopathological representative picture showing arteriogenesis of adductor muscles from four different groups using α-SMA staining, with 400× magnification. Arteriogenesis assessment after hindlimb ischemia (HLI) and administration of exosomes (A), conditioned media (B) and phosphate-buffered saline (PBS) (C), and non-HLI sham-operated control (D) are shown with arteriole lumen which indicated by arrows. Scale bar is equivalent to 50 µm.

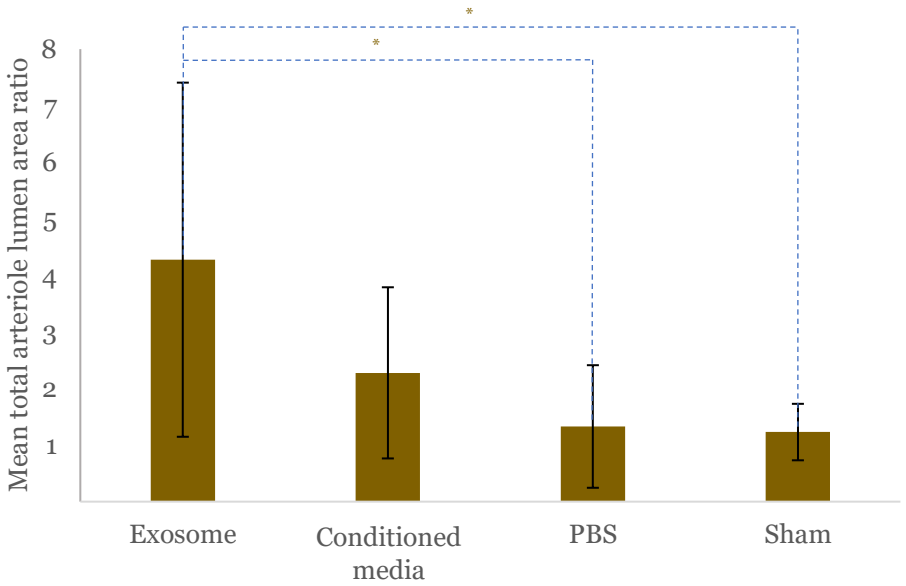

Figure 5. Comparison of mean total arteriole lumen area ratio between exosome, conditioned media, PBS, and sham-operated groups. The ratio was calculated by comparing the total CD31-positive cells in the gastrocnemius muscle of the limb with ligation as hindlimb ischemia (HLI) model compared to contralateral limb without ligation. Black vertical lines depict standard deviation of mean from each group. The asterisk (*) indicates statistical significance.

There was a significant difference in the degree of clinical necrosis between the four intervention groups (p=0.005). Further analysis shows statistically insignificant results for the exosome group compared to the conditioned media (p=0.725) and sham-operated group (p=0.510). However, there was a significantly lower degree of clinical necrosis between the exosome and PBS groups (p=0.005).

The degree of necrosis was also evaluated microscopically in all study groups using histopathological assessment, with results presented in **Figure 8** and **Figure 9**. Histopathological analysis utilized hematoxylin-eosin staining of gastrocnemius muscle preparations, and the Carter scoring system was applied. In the exosome group, scattered mononuclear cells and rare necrotic fibers (Grade 2) were observed (**Figure 8**). Necrotic cells displayed brighter cytoplasmic staining, centrally located nuclei, and infiltration by mononuclear inflammatory cells. In contrast, both the conditioned media and PBS groups exhibited prominent infiltration, including polymorphonuclear cells (PMNs), and moderate multifocal fiber necrosis (Grade 5) (**Figure 8**). The conditioned media group showed brighter cytoplasmic staining, centrally located nuclei, reduced cell size, vacuolization, and diffuse inflammatory infiltration, including PMNs, indicating more severe necrosis (**Figure 8**). Additionally, necrotic cells were partially replaced by fat cells. The PBS group demonstrated similar signs but with more extensive inflammatory cell infiltration and less distinct cell boundaries due to reduced cell size. The sham-operated group exhibited the lowest degree of necrosis, characterized by minimal local infiltration of mononuclear cells (Grade 1) (**Figure 8**). The muscle fibers appeared intact, with normal-sized cells, pinkish cytoplasm, peripherally located nuclei, and only minimal mononuclear cell infiltration.

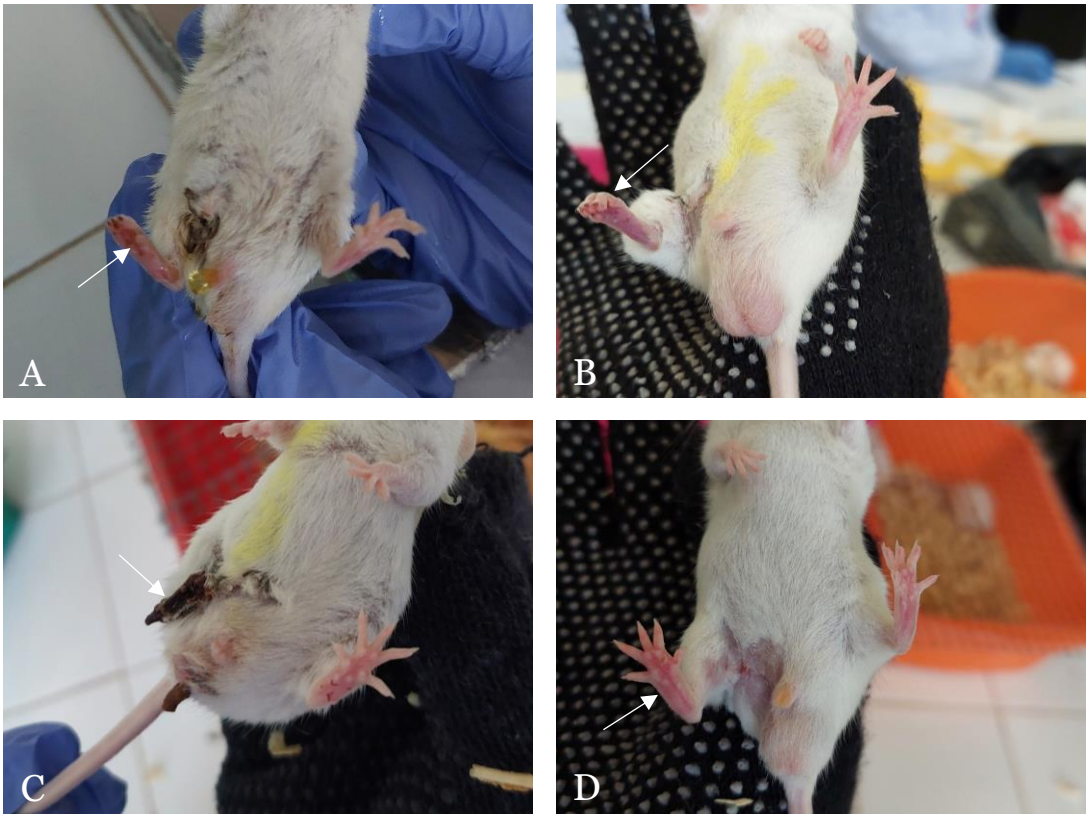

Figure 6. Representative pictures of clinical degree of necrosis among study groups. The clinical necrosis was assessed on the right ligated limb (arrow) after hindlimb ischemia (HLI) following administration of exosome, conditioned media, PBS, and non-HLI sham-operated. In the exosome group (A), black discoloration is observed, particularly on the nails, accompanied by a darker red hue in the ligated limb. The conditioned media group (B) shows more prominent black nail discoloration and a darker red limb compared to the exosome group. In the PBS group (C), Grade 4 necrosis is evident in the ligated limb, progressing to autoamputation. In contrast, the sham-operated group (D) exhibits no signs of necrosis, with white nails and a pink limb color similar to the control limb.

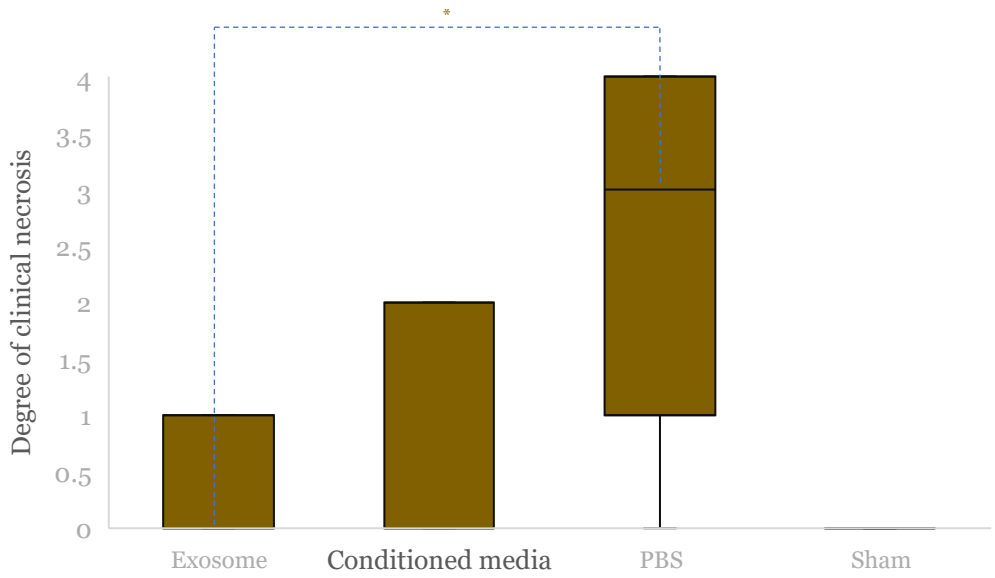

Figure 7. Median clinical degree of necrosis after hindlimb ischemia (HLI) and administration of exosome, conditioned media and PBS, and non-HLI sham-operated control was compared. Boxes indicate interquartile range, black horizontal lines are median of each group (the values are 0 from exosome, conditioned media, and sham-operated group), and black vertical lines are minimum to maximum value. The asterisk (*) indicates statistical significance.

A significant difference in the mean of necrosis scores was observed among the groups (exosome vs. conditioned media vs. PBS vs. sham; 3.71±1.6 vs 4.67±2.58 vs 6.86±3.39 vs 1.29±0.76; p=0.002) (**Figure 9**). Post hoc analysis (Games-Howell) showed that necrosis scores in the exosome group were lower than in the conditioned media and PBS groups but not statistically significant (p=0.86 and p=0.193, respectively) (**Figure 9**). The sham group had the lowest degree of necrosis.

Differential expression of miRNAs

Differential expression of miRNAs (1.5-fold changes), both upregulated and downregulated, is depicted in **Table 2**. In the exosome group, mmu-mir-15b and mmu-miR-599 were the most downregulated and upregulated compared to conditioned media, respectively, while mmu-miR-92a and mmu-let-7f were most downregulated and upregulated compared to the PBS group, respectively (**Table 2**).

Table 2. Comparisons of miRNA expressions between study groups based on NanoString analysis

Comparison	miRNAs	Fold changes	p-value	Adjusted p-value
Exosome vs conditioned media				
	mmu-mir-15b	1.56	0.034	0.884
	mmu-miR-599	-2.29	0.009	0.884
	mmu-miR-542-3p	-1.77	0.032	0.884
	mmu-miR-384-3p	-1.53	0.048	0.884
Exosome vs PBS				
	mmu-let-7f	1.74	0.021	0.981
	mmu-mir-15b	1.63	0.039	0.981
	mmu-miR-344	-1.75	0.007	0.981
	mmu-miR-1941-3p	-1.54	0.019	0.981
	mmu-miR-599	-1.72	0.030	0.981
	mmu-miR-1953	-1.59	0.032	0.981
	mmu-miR-92a	-1.98	0.037	0.981
	mmu-mir-511	-1.63	0.038	0.981
	mmu-mir-127	-1.95	0.042	0.981
	mmu-mir-1981	-1.68	0.044	0.981
Exosome vs sham-operated				
	mmu-mir-15b	1.88	0.018	0.995
	mmu-miR-707	1.82	0.028	0.995
	mmu-let-7f	1.64	0.032	0.995
	mmu-miR-125b-5p	-2.94	0.000	0.144

Comparison	miRNAs	Fold changes	*p*-value	Adjusted *p*-value
	mmu-miR-378	-4.30	0.001	0.227
	mmu-mir-99a	-1.86	0.005	0.610
	mmu-miR-720	-2.30	0.009	0.815
	mmu-miR-486	-3.06	0.017	0.995
	mmu-miR-133a	-2.51	0.021	0.995
	mmu-miR-181a	-1.76	0.043	0.995
Conditioned media vs PBS				
	mmu-mir-130a	1.55	0.004	0.962
	mmu-miR-1906	1.61	0.007	0.962
	mmu-mir-205	1.63	0.008	0.962
	mmu-miR-666-5p	2.59	0.011	0.962
	mmu-mir-1964	1.61	0.014	0.962
	mmu-miR-582-5p	1.54	0.023	0.962
	mmu-mir-203	1.62	0.023	0.962
	mmu-mir-500	2.03	0.045	0.962
	mmu-miR-1904	1.61	0.045	0.962
	mmu-miR-1931	1.55	0.048	0.962
	mmu-mir-664	-1.73	0.016	0.962
	mmu-mir-698	-1.79	0.026	0.962
	mmu-miR-693-5p	-1.79	0.026	0.962
	mmu-miR-1900	-1.51	0.030	0.962
	mmu-mir-18b	-1.73	0.041	0.962
	mmu-miR-1960	-1.89	0.043	0.962
Conditioned media vs sham-operated				
	mmu-miR-26a	1.55	0.001	0.299
	mmu-mir-130a	1.73	0.003	0.299
	mmu-mir-871	1.75	0.007	0.299
	mmu-mir-1964	1.64	0.008	0.299
	mcmv-miR-M95-1-3p	1.68	0.013	0.299
	mmu-miR-19b	1.68	0.013	0.299
	mmu-miR-384-3p	1.74	0.013	0.299
	mmu-mir-1199	1.89	0.014	0.299
	mmu-mir-674	1.62	0.015	0.299
	mmu-miR-707	1.67	0.017	0.299
	mmu-mir-670	1.51	0.018	0.299
	mmu-mir-297c	1.60	0.018	0.299
	mmu-miR-466d-5p	1.72	0.019	0.299
	mmu-miR-195	1.83	0.019	0.299
	mmu-miR-2133	1.51	0.019	0.299
	mmu-miR-466f-5p	1.85	0.020	0.299
	mmu-miR-1894-3p	2.00	0.023	0.299
	mmu-mir-376c	1.57	0.023	0.299
	mmu-miR-761	1.84	0.023	0.299
	mmu-mir-467b	1.60	0.025	0.299
	mmu-miR-696	2.30	0.025	0.299
	mmu-mir-302a	1.67	0.027	0.299
	mmu-miR-1931	1.75	0.027	0.299
	mmu-miR-568	1.95	0.029	0.299
	mmu-mir-361	1.68	0.029	0.299
	mmu-miR-125b-5p	-2.78	0.002	0.299
	mmu-miR-181a	-1.77	0.009	0.299
	mmu-miR-378	-3.71	0.011	0.299
	mmu-miR-30c	-2.30	0.013	0.299
	mmu-miR-720	-2.78	0.023	0.299
	mmu-miR-151-5p	-2.07	0.024	0.299
	mmu-miR-199a-3p	-1.86	0.026	0.299
	mmu-miR-196a	-3.09	0.028	0.299
	mmu-mir-23a	-1.94	0.034	0.299
	mmu-miR-1	-3.77	0.034	0.299
	mmu-let-7d	-2.37	0.040	0.299
	mmu-mir-22	-2.48	0.046	0.307
	mmu-miR-1937c	-1.63	0.048	0.307

PBS: phosphate-buffered saline

The mmu-mir-378 and mmu-mir-15b were the most downregulated and upregulated miRNA, respectively, compared to the sham-operated group (**Table 2**). Although these

differences were statistically significant, the adjusted *p*-values were not significant. Detailed comparisons of miRNA expressions between study groups are presented in **Table 2**.

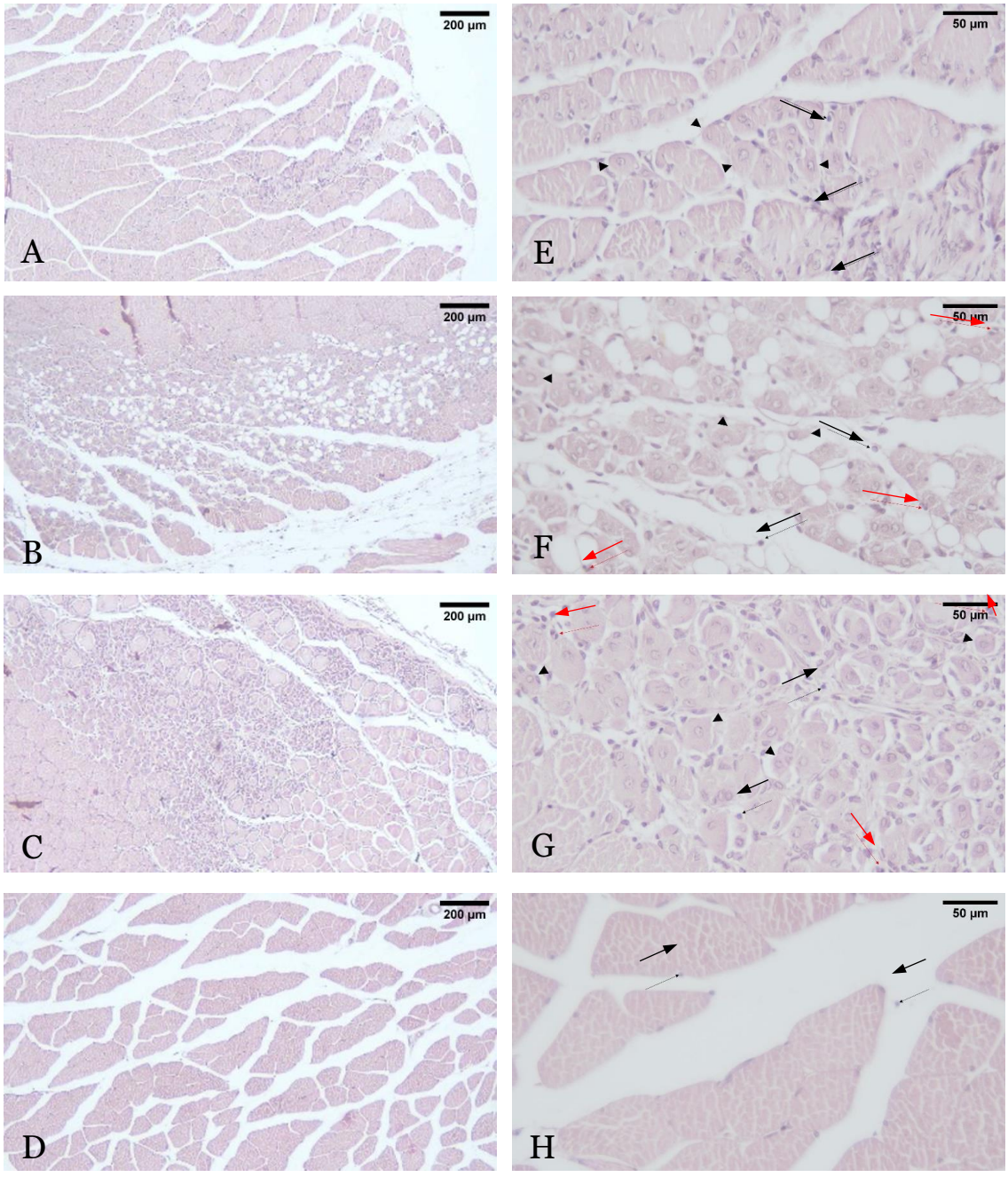

Figure 8. The histopathological necrosis with hematoxylin-eosin staining on 100x (A-D) and 400× (E-H) magnification after administration of exosome (A and E), conditioned media (B and F), PBS (C and G), and sham-operated (D and H) intervention. Arrowhead shows necrotic muscle cells, black arrow shows mononuclear cell infiltration, and red arrow shows polymorphonuclear cell infiltration.

miRNA expression profiles

Differential expression of miRNA was identified using the nSolver Analysis Software (V4.0). All fold changes (FC) are represented in log 2 scale (log FC). Statistically significant miRNAs were selected with $|FC| \geq 1.5$ ($p<0.05$). To evaluate the function of the significantly different miRNAs, pathway and Gene Ontology analysis in particular biological process target enrichment analysis was done using Metascape. As previously known, gene product carries out a molecular-level process or activity in a specific location relative to the cell, and this molecular process is involved in a larger biological objective comprised of multiple molecular-level processes. The latter is the focus of the biological process enrichment analysis we conducted.

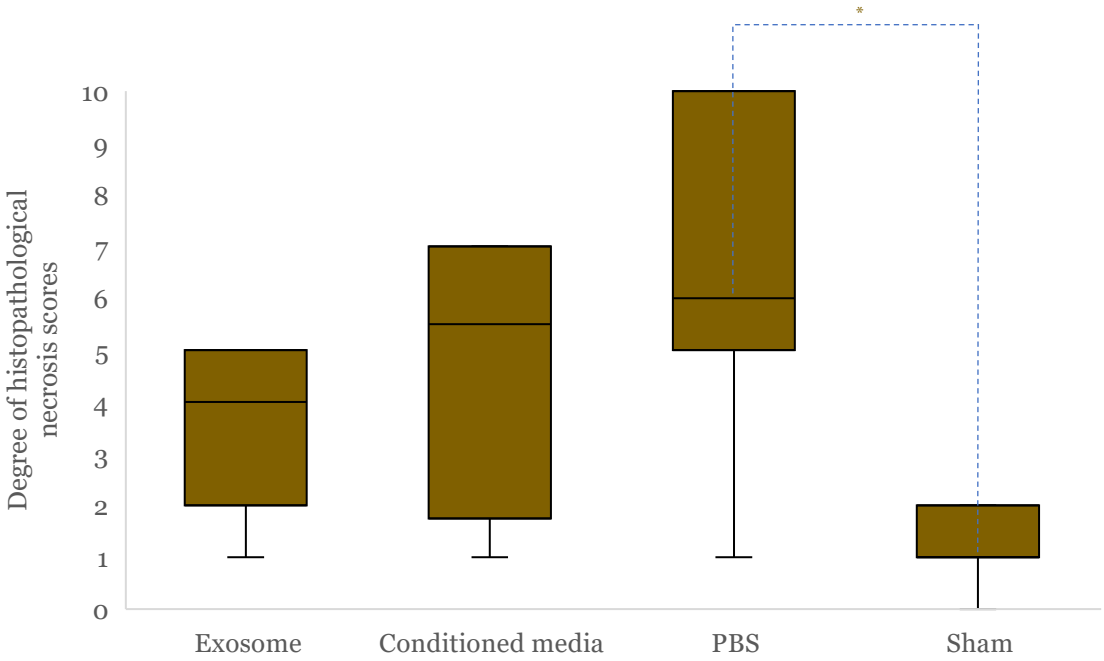

Figure 9. Comparison of median histopathological necrosis score after hindlimb ischemia (HLI) and administration of exosome, conditioned media and PBS, and non-HLI sham-operated control. The boxes indicate interquartile range, black horizontal lines are median of each group (the value is 1 from sham-operated group), and black vertical lines are minimum to maximum value. The asterisk (*) indicates statistical significance.

The biological process target enrichment analysis of the exosome (**Figure 10A**) and conditioned media group (**Figure 10B**) in comparison to the sham-operated group suggested there was enrichment in biological process related to arteriogenesis and angiogenesis like regulation of phosphatidylinositol 3-kinase/protein kinase B signal transduction and enzyme-linked receptor protein signaling pathway. Moreover, there was enrichment in biological processes related to energy regulation (regulation of generation of precursor metabolites and energy; hexose metabolic process), which might affect cell proliferation due to the availability of energy reserves.

The enrichment analysis of the exosome and conditioned media groups, in comparison to the PBS group, are presented in **Figure 10C** and **10D**, respectively. Based on pathway and biological process enrichment analysis, exosome and conditioned media groups had several enrichments related to the arteriogenesis and angiogenesis processes. The biological pathways that could potentially affect neovascularization and limb necrosis are the TGF-β signaling pathway, the ubiquitin-proteasome system, and the tyrosine kinase receptors. Meanwhile, gene expression regulation and cell proliferation are dominantly affected when comparing conditioned media to PBS. Our data suggested there was enrichment in positive regulation of protein localization and calcium ion transmembrane transport between the exosome and conditioned media group (**Figure 10E**).

In silico analysis of miRNA pathways involving mmu-mir-15b and mmu-let-7f

Profiling miRNA presented in **Table 2** revealed that mmu-mir-15b and mmu-let-7f relatively consistently upregulated in the exosome group. Further analysis of these miRNAs using miRPath v4.0 (TarBase v8.0 database) revealed significant involvement in several pathways, including the FoxO signaling pathway, hypoxia-induced factor 1 (HIF-1) signaling pathway, PI3K/AKT signaling pathway, fluid shear stress and atherosclerosis, and VEGF signaling pathway according to the KEGG Database (**Figure 11**).

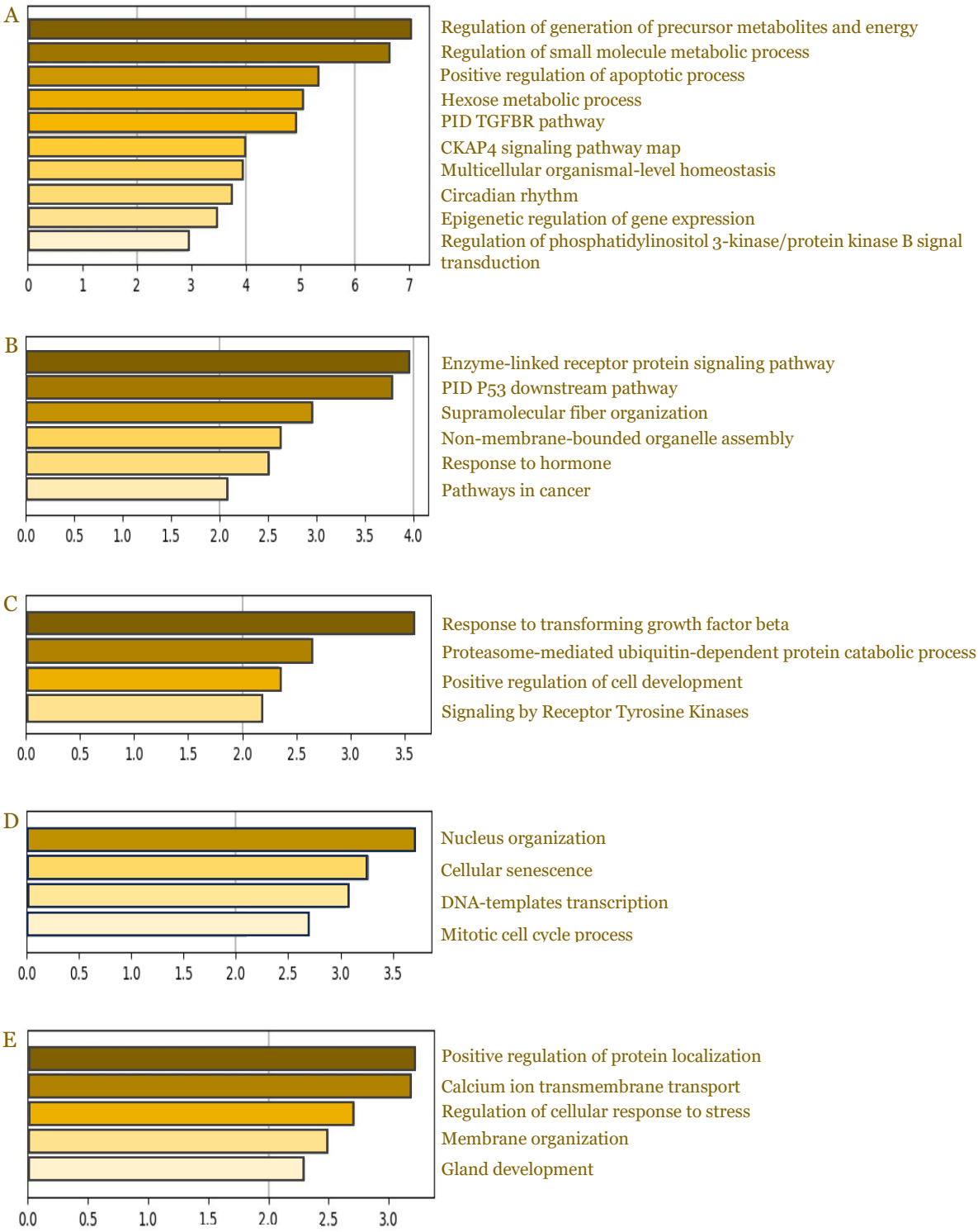

Figure 10. Results of Gene Ontology analysis. The figures show the biological process target enrichment analysis of exosome group compared to sham-operated group (A), conditioned media compared to sham-operated (B), exosome compared to PBS (C), conditioned media compared to PBS (D), and exosome group compared to conditioned media group (E).

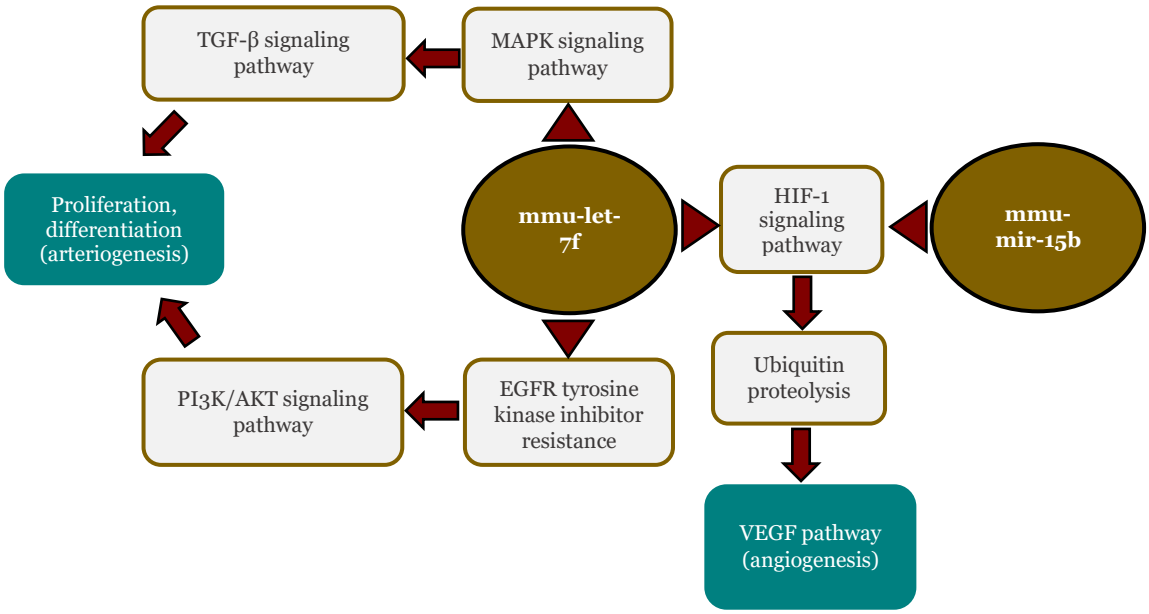

Figure 11. In silico analysis of mmu-mir-15b and mmu-let-7f using miRPath.

Analysis of VEGF mRNA expression

The VEGF mRNA expression in the adductor muscles of the ligated leg was also assessed in this study. Our study indicated that animals within exosome group had a decreased VEGF mRNA expression compared to animals within conditioned media, PBS, and sham-operated groups (0.35±0.18 vs 0.77±0.68 vs 0.95±0.14 vs 1.82±2.17; p=0.361), although the difference was not statistically significant (**Figure 12**).

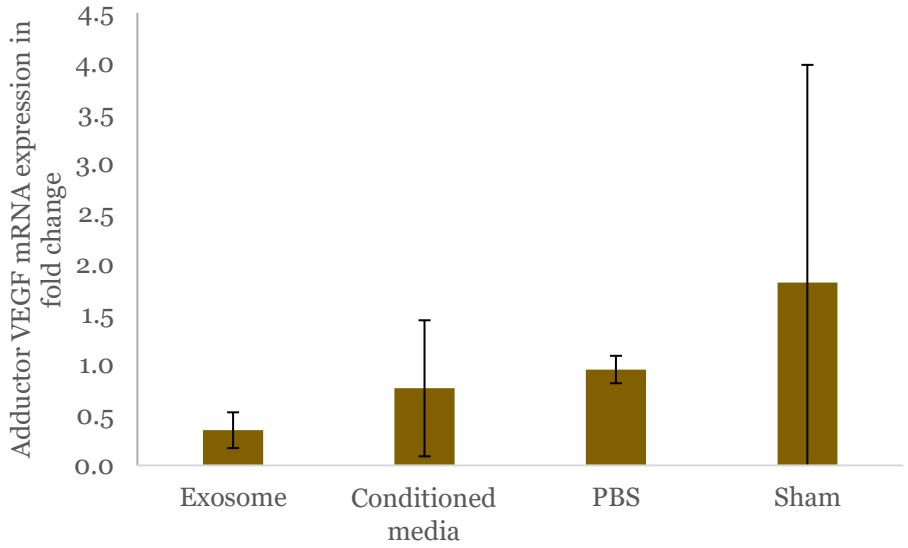

Figure 12. Comparison of vascular endothelial growth factor (VEGF) mRNA expression in adductor muscles among study groups shown by fold changes. Mean value of each group is represented by bars, with its standard deviation denoted by black vertical line. The cycle threshold (CT) value for the gene was normalized against the CT value of GAPDH to obtain the delta CT value (ΔCt). Subsequently, the delta CT value is subtracted by CT value of sham-operated group, which serves as the control, resulting in ΔΔCt, and the fold change is obtained by $2^{-\Delta\Delta Ct}$ formula.

Discussion

In this study, we assessed how exosomes derived from HUVECs impact a hindlimb ischemia mice model. Our findings demonstrated that administering HUVECs-derived exosomes directly into an ischemic area could increase capillary density, arteriole area, and reduce necrotic stage. These effects might be mediated by several possible mechanisms, including energy regulation and

activation of the PI3K/AKT signaling pathway, TGF-β signaling pathway, ubiquitin-proteasome system, and tyrosine kinases receptors. To our knowledge, this is the first study that assesses the effect of exosome HUVEC in mice models of hindlimb ischemia.

Exosomes are nanoscale vesicles with a size range of 30–100 nm, containing various molecules [26] and their therapeutic potential stems from their miRNA content [17]. Once reaching target cells, exosomes can initiate signaling by directly interacting with extracellular receptors, fusing directly with the plasma membrane, or being internalized into target cells [27]. A previous study showed that HUVECs-derived exosomes can be internalized by endothelial cells [28]. This may occur because exosomes are preferentially internalized by the cell type from which they were initially secreted [29,30].

Exosomes derived from human umbilical cord mesenchymal stem cells can come from umbilical cord blood, Wharton's jelly, or HUVECs. Wharton's jelly tissue produces the highest allogeneic mesenchymal stem cell components [20]. HUVECs have more CD146 adhesion molecules, which play a role in the angiogenesis process by inducing activation of P38 and ERK1/2 signaling pathways involved in vascular endothelial growth factor receptor 2 (VEGFR2) signaling, indicating that CD146 can act as a coreceptor for VEGFR2 [21,31]. In vitro study with matrigel tube formation assay showed better tube formation ability and length in HUVECs compared to Wharton's jelly [21]. The expression of the notch ligand jagged1 (JAG1) was also higher in HUVECs compared to Wharton's jelly, which is important for blood vessel maturation [21]. Exosomes derived from HUVECs can increase proliferation (based on MTT analysis) and migration of endothelial cells (assessed using scratch wound assay) [28]. Therefore, it can be assumed that exosomes derived from HUVECs contain higher levels of angiogenesis and arteriogenesis factors.

Some miRNAs, including miR-126-3p, have been documented to reach their peak expression at day 1 after administration and persisting out to day 3 [32], therefore we decided to perform the miRNA profiling one day after exosome injection. Meanwhile, innate arteriogenesis was revealed to occur 7–14 days after ischemia induction in HLI murine model, supported by an increase in arterial lumen area [33]. Therefore, the mice were sacrificed on the seventh day to assess neovascularization.

While no animal models can perfectly simulate PAD in humans, mouse hindlimb ischemia models represent some of its key features (angiogenesis, arteriogenesis, and alteration of skeletal muscle composition). The murine hindlimb ischemia model shows a similar neovascularization pattern to that of PAD patients, with a limited collateral network resembling the human vascular system [34]. In particular, the Balb/c mice demonstrated a genetic composition that results in a slow recovery of blood perfusion believed to closely mimic the situation in patients with PAD [35]. Moreover, the mice model is an ideal choice for accurately profiling the miRNAs and their biological processes due to their identical genetic background, with a 99% similarity with the human genome [36].

Based on our in silico analysis of miRNA pathways (**Figure 10**), it was revealed that the target genes of differentially expressed miRNA between the exosome vs the sham-operated group showed enrichment in the regulation of PI3K/AKT. Therefore, this indicated that the PI3K/AKT signaling pathway confirmed in the mice model of acute myocardial infarction may also affect arteriogenesis and angiogenesis in the context of HLI.

Moreover, biological process enrichment in the regulation of generation of precursor metabolites and energy might be related to angiogenesis due to how endothelial cells both produce and consume energy in order to drive cell proliferation and migration, maintain their structural integrity, and adapt to environmental changes as they transition from a quiescent to an angiogenic phenotype [37]. Disruption in energy regulation, particularly glucose utilization and mitochondrial respiration, has been linked to severe tissue necrosis and autoamputation [38]. Modulation of the enzyme-linked receptor protein signaling pathway in response to conditioned media treatment, such as VEGF signaling pathway and VEGF receptor signaling pathway, is also beneficial for arteriogenesis and angiogenesis, as shown in the improvement of lumen area, capillary density, and necrotic stage between the conditioned media vs the sham-operated group.

Compared to the PBS group, HUVECs-derived exosomes increased arteriogenesis, angiogenesis, and improved necrotic stage through several possible mechanisms, including TGF-β signaling, ubiquitin-proteasome system, and the tyrosine kinase receptors. TGF-β signaling has been known to affect vascular function, including angiogenesis [39]. A previous study has shown that the TGF-β1 signaling pathway may act as muscle protection against ischemic injury and prevent necrosis by inducing a fast angiogenic switch [40]. The ubiquitin-proteasome system also plays a critical role in fine-tuning the function of core pro-angiogenic proteins, such as VEGF, VEGFR-2, angiogenic signaling proteins, including PLCγ1 and PI3K/AKT pathway, as well as other non-VEGF angiogenic pathways [41]. Receptor tyrosine kinase, particularly through the VEGF and tie receptors, plays a pivotal role in angiogenesis [42].

VEGF is also important for the arteriogenesis process [43]. In arteriogenesis, VEGF activation from extracellular signal-regulating kinase 1/2 (ERK1/2) can induce the proliferation of endothelial cells, tissue formation, and increased lumen size, which ultimately stimulates arteriogenesis [44]. In arteriogenesis, the isoforms ERK1 and ERK2 play distinct roles. ERK1 is involved in the regulation of macrophage infiltration following ischemia, whereas ERK2 is responsible for the regulation of endothelial cell proliferation and eNos expression. Additionally, both isoforms are involved in the regulation of endothelial cell migration [45]. Impaired ERK1/2 activity in endothelial cells leads to reduced VEGF production, consequently decreasing arteriogenesis [44]. Compared to PBS, conditioned media increased arteriogenesis and angiogenesis might be influencing the biological process “mitotic cell cycle” due to its role in governing cell proliferation, a fundamental mechanism underlying the formation and remodeling of blood vessels.

Two miRNAs, mmu-mir-15b and mmu-let-7f, were consistently upregulated in the exosome group compared to other groups. Further analysis of these miRNAs showed significant involvement in the HIF-1 signaling pathway, PI3K/AKT signaling pathway and VEGF signaling pathway. These pathways are well-known and involved in arteriogenesis and angiogenesis. Moreover, the ischemic condition activates HIF-1, leading to an increase in growth factors such as VEGF, which induces angiogenesis [46].

Based on the results of biological processes analysis performed on exosomes compared to conditioned media, there was enrichment in calcium transmembrane transport. In general, calcium is recognized as an ion that plays a crucial role in various biological processes, including cellular signaling. In the context of angiogenesis, calcium can influence diverse aspects such as endothelial cell proliferation, endothelial cell migration, and capillary tube formation [47].

Not all of the biological processes mentioned above directly affect the mechanism of limb necrosis, but they may contribute indirectly through the promotion of neovascularization. The severity of necrosis is consistent with the ability to perform a substantial blood flow recovery response, and poor perfusion is associated with an increased rate of endothelial cell apoptosis [48,49].

The analysis of VEGF mRNA expression in the adductor muscle revealed the lowest levels in the exosome group compared to the conditioned media, PBS, and sham groups. The higher VEGF mRNA expression observed in the PBS group suggests a compensatory response to more severe ischemic conditions. VEGF, a key endothelial growth factor, plays a critical role in both physiological and pathological angiogenesis. Under normal conditions, VEGF protects against apoptosis, but its expression can significantly increase in response to hypoxia due to stabilization of its mRNA in the 5' untranslated regions (UTR), coding region, and 3'UTR [50,51].

In hypoxic conditions, elevated VEGF mRNA expression is often linked to increased HIF-1 activity, as VEGF is a direct target of HIF-1α [52]. Notably, the sham-operated group exhibited the highest VEGF mRNA expression, which may be attributed to inflammation resulting from the treatment. Inflammation, a natural response to injury, aims to repair tissue but can also exacerbate damage and induce hypoxia, leading to increased production of angiogenic factors such as VEGF [53].

There are several limitations in this study. First, we were unable to confirm the flow of the ischemic limb by laser doppler perfusion imaging due to unavailability of the facility. Instead, we assessed perfusion indirectly through the measurement of CD31, a marker associated with vascularization. Second, the experiments represent an experimental acute-phase hindlimb

ischemia without atherosclerosis, however, this model is widely accepted in CLTI research for studying the concept of neovascularization. Third, we only conducted in silico analysis, therefore further signaling pathway validation is still required.

Conclusion

Exosomes derived from HUVECs could increase neovascularization and decrease necrosis in hindlimb ischemia mice model, potentially by modulating several possible mechanisms, including energy regulation, activation of the PI3K/AKT and TGF-β signaling pathways, ubiquitin-proteasome system, tyrosine kinases receptor signaling, and calcium transmembrane transport. HUVEC exosomes are generally associated with lower VEGF mRNA expression, which may indicate a more effective compensatory mechanism under ischemic conditions. These findings may offer a starting point for further investigation into HUVECs-derived exosomes, which could help assess their potential as a new translational therapy for CLTI in humans.

Ethics approval

The study was conducted in compliance with the guidelines of Medical and Health Research Ethics Committee (MHREC) of Faculty of Medicine, Universitas Gadjah Mada – Dr. Sardjito General Hospital (Forum for Ethical Review Committees in Asia and Western Pacific / FERCAP) for research involving animal. Ethical approval was obtained from MHREC under clearance no. KE/FK/1146/EC/2022 on September 7, 2022, confirming adherence to the ethical principles of Declaration of Helsinki 2008.

Acknowledgments

We extend our heartfelt gratitude to Afif Ramadhan, Hariadi, Jessica Eve, and Atika Sari Dewi for their technical assistance in study execution and data analysis. We sincerely thank Nur Arfian and Fauziyatul Munawaroh from the anatomy laboratory, PT. Dermama, the histopathologist, and Medical Research Ethics Committee of Gadjah Mada University's Faculty of Medicine, Public Health, and Nursing for their invaluable contributions to this study, all of whom approved its inclusion.

Competing interests

The authors declare no potential conflict of interest with respect to the research, authorship, and/or publication of this article.

Funding

Work in our laboratory including miRNA profiling was supported by Sistem Informasi Manajemen Penelitian dan Pengabdian Kepada Masyarakat (SIMLITABMAS) 2022 grant number 089/E5/PG.02.00.PT/2022 and 1889/UN1/DITLIT/Dit-Lit/PT.01.03/2022.

Underlying data

All data underlying the results are available as part of the article and no additional source data are required.

How to cite

Ismail MT, Anggrahini DW, Haryana SM, Setianto BY. HUVECs-derived exosomes increase neovascularization and decrease limb necrosis in hindlimb ischemia. Narra J 2024; 4 (3): e1358 - http://doi.org/10.52225/narra.v4i3.1358.

References

1. Sidawy AN, Perler BA. Rutherford's vascular surgery and endovascular therapy. 10th Edition. Philadelphia: Elsevier; 2023.
2. Vitalis A, Lip GYH, Kay M, *et al.* Ethnic differences in the prevalence of peripheral arterial disease: A systematic review and meta-analysis. Expert Rev Cardiovasc Ther 2017;15(4):327-338.

3. Dhaliwal G, Mukherjee D. Peripheral arterial disease: Epidemiology, natural history, diagnosis and treatment. Int J Angiol 2007;16(2):36-36.
4. Fowkes FGR, Rudan D, Rudan I, *et al.* Comparison of global estimates of prevalence and risk factors for peripheral artery disease in 2000 and 2010: A systematic review and analysis. Lancet 2013;382(9901):1329-1340.
5. Van RNS, Hensing T, Santema TB, *et al.* Outcomes of conservative treatment in patients with chronic limb threatening ischaemia: A systematic review and meta-analysis. Eur J Vasc Endovasc Surg 2021;62(2):214-224.
6. Baubeta FE, Andersson M, Thuresson M, *et al.* Amputation rates, mortality, and pre-operative comorbidities in patients revascularised for intermittent claudication or critical limb ischaemia: A population based study. J Vasc Surg 2017;66(5):1627-1628.
7. Reinecke H, Unrath M, Freisinger E, *et al.* Peripheral arterial disease and critical limb ischaemia: Still poor outcomes and lack of guideline adherence. Eur Heart J 2015;36(15):932-938.
8. Conte MS, Bradbury AW, Kolh P, *et al.* Global vascular guidelines on the management of chronic limb-threatening ischemia. Eur J Vasc Endovasc Surg 2019;58(1):S1-S109.e33.
9. Verwer MC, Wijnand JGJ, Teraa M, *et al.* Long term survival and limb salvage in patients with non-revascularisable chronic limb threatening ischaemia. Eur J Vasc Endovasc Surg 2021;62(2):225-232.
10. Arango-Rodríguez ML, Mateus LC, Sossa CL, *et al.* A novel therapeutic management for diabetes patients with chronic limb-threatening ischemia: Comparison of autologous bone marrow mononuclear cells versus allogenic Wharton jelly-derived mesenchymal stem cells. Stem Cell Res Ther 2023;14:221.
11. Liang TW, Jester A, Motaganahalli RL, *et al.* Autologous bone marrow mononuclear cell therapy for critical limb ischemia is effective and durable. J Vasc Surg 2016;63(6):1541-1545.
12. Teraa M, Sprengers RW, Schutgens REG, *et al.* Effect of repetitive intra-arterial infusion of bone marrow mononuclear cells in patients with no-option limb ischemia: The randomized, double-blind, placebo-controlled Rejuvenating Endothelial Progenitor Cells via Transcutaneous Intra-arterial Supplementation (JUVENTAS) trial. Circulation 2015;131(10):851-860.
13. Lukomska B, Stanaszek L, Zuba-Surma E, *et al.* Challenges and controversies in human mesenchymal stem cell therapy. Stem Cells Int 2019;2019:1-10.
14. Caicedo D, Devesa P, Arce VM, *et al.* Chronic limb-threatening ischemia could benefit from growth hormone therapy for wound healing and limb salvage. Ther Adv Cardiovasc Dis 2018;12(2):53-72.
15. Pérez-Cremades D, Cheng HS, Feinberg MW. Noncoding RNAs in critical limb ischemia. Arterioscler Thromb Vasc Biol 2020;40(3):523-533.
16. Dilsiz N. Role of exosomes and exosomal microRNAs in cancer. Future Sci OA 2020;6(4):FSO465.
17. Abbaszadeh H, Ghorbani F, Derakhshani M, *et al.* Human umbilical cord mesenchymal stem cell-derived extracellular vesicles: A novel therapeutic paradigm. J Cell Physiol 2020;235(2):706-717.
18. Zhang Y, Liu Y, Liu H, *et al.* Exosomes: Biogenesis, biologic function and clinical potential. Cell Biosci 2019;9(1):19.
19. Mathiyalagan P, Liang Y, Kim D, *et al.* Angiogenic mechanisms of human $CD34^+$ stem cell exosomes in the repair of ischemic hindlimb. Circ Res 2017;120(9):1466-1476.
20. Arutyunyan I, Elchaninov A, Makarov A, *et al.* Umbilical cord as prospective source for mesenchymal stem cell-based therapy. Stem Cells Int 2016;2016(1):6901286.
21. Xu L, Zhou J, Liu J, *et al.* Different angiogenic potentials of mesenchymal stem cells derived from umbilical artery, umbilical vein, and wharton's jelly. Stem Cells Int 2017;2017:1-15.
22. Liu W, Feng Y, Wang X, *et al.* Human umbilical vein endothelial cells-derived exosomes enhance cardiac function after acute myocardial infarction by activating the PI3K/AKT signaling pathway. Bioengineered 2022;13(4):8850-8865.
23. Wang L, Chen Z, Li Y, *et al.* Optical coherence tomography angiography for noninvasive evaluation of angiogenesis in a limb ischemia mouse model. Sci Rep 2019;9:5980.
24. Wang J, Guo Y, Xu D, *et al.* The immunolocalization of cluster of differentiation 31, phalloidin and alpha smooth muscle actin on vascular network of normal and ischemic rat brain. Sci Rep 2022;12(1):22288.
25. Carter WO, Bull C, Bortolon E, *et al.* A murine skeletal muscle ischemia-reperfusion injury model: Differential pathology in BALB/c and DBA/2N mice. J Appl Physiol 1998;85(5):1676-1683.
26. Thongboonkerd V. Roles for exosome in various kidney diseases and disorders. Front Pharmacol 2020;10:1655.
27. Gurung S, Perocheau D, Touramanidou L, *et al.* The exosome journey: From biogenesis to uptake and intracellular signalling. Cell Commun Signal 2021;19(1):47.
28. Hu H, Jiang C, Li R, *et al.* Comparison of endothelial cell- and endothelial progenitor cell-derived exosomes in promoting vascular endothelial cell repair. Int J Clin Exp Pathol 2019;12(7):2793-2800.

29. Sancho-Albero M, Navascués N, Mendoza G, *et al.* Exosome origin determines cell targeting and the transfer of therapeutic nanoparticles towards target cells. J Nanobiotechnology 2019;17(1):16.
30. Jurgielewicz BJ, Yao Y, Stice SL. Kinetics and specificity of HEK293T extracellular vesicle uptake using imaging flow cytometry. Nanoscale Res Lett 2020;15(1):170.
31. Joshkon A, Heim X, Dubrou C, *et al.* Role of CD146 (MCAM) in physiological and pathological angiogenesis—contribution of new antibodies for therapy. Biomedicines 2020;8(12):633.
32. Cao WJ, Rosenblat JD, Roth NC, *et al.* Therapeutic angiogenesis by ultrasound-mediated MicroRNA-126-3p Delivery. Arterioscler Thromb Vasc Biol 2015;35(11):2401-2411.
33. Andersen NJ, Boguslawski EA, Naidu AS, *et al.* Anthrax toxin receptor 1 is essential for arteriogenesis in a mouse model of hindlimb ischemia. PL0S One 2016;11(1):e0146586.
34. Heuslein JL, Gorick CM, Price RJ. Epigenetic regulators of the revascularization response to chronic arterial occlusion. Cardiovasc Res 2019;115(4):701-712.
35. Aref Z, De Vries MR, Quax PHA. Variations in surgical procedures for inducing hindlimb ischemia in mice and the impact of these variations on neovascularization assessment. Int J Mol Sci 2019;20(15):3704.
36. Vandamme T. Use of rodents as models of human diseases. J Pharm Bioallied Sci 2014;6(1):2.
37. Du W, Ren L, Hamblin MH, *et al.* Endothelial cell glucose metabolism and angiogenesis. Biomedicines 2021;9(2):147.
38. Dunn LL, Kong SMY, Tumanov S, *et al.* Hmox1 (Heme oxygenase-1) protects against ischemia-mediated injury via stabilization of HIF-1α (hypoxia-inducible factor-1α). Arterioscler Thromb Vasc Biol 2021;41(1):317-330.
39. Goumans MJ, Ten Dijke P. TGF-β signaling in control of cardiovascular function. Cold Spring Harb Perspect Biol 2018;10(2):a022210.
40. Cavallari C, Ranghino A, Tapparo M, *et al.* Serum-derived extracellular vesicles (EVs) impact on vascular remodeling and prevent muscle damage in acute hindlimb ischemia. Sci Rep 2017;7(1):8180.
41. Rahimi N. The ubiquitin-proteasome system meets angiogenesis. Mol Cancer Ther 2012;11(3):538-548.
42. Jeltsch M, Leppanen VM, Saharinen P, *et al.* Receptor Tyrosine Kinase-Mediated Angiogenesis. Cold Spring Harb Perspect Biol 2013;5(9):a009183-a009183.
43. Moraes F, Paye J, Mac Gabhann F, *et al.* Endothelial cell–dependent regulation of arteriogenesis. Circ Res 2013;113(9):1076-1086.
44. Lanahan AA, Lech D, Dubrac A, *et al.* PTP1b is a physiologic regulator of vascular endothelial growth factor signaling in endothelial cells. Circulation 2014;130(11):902-909.
45. Ricard N, Zhang J, Zhuang ZW, *et al.* Isoform-specific roles of ERK1 and ERK2 in arteriogenesis. Cells 2019;9(1):38.
46. Simon F, Oberhuber A, Floros N, *et al.* Pathophysiology of chronic limb ischemia. Gefässchirurgie 2018;23(S1):13-18.
47. Moccia F, Negri S, Shekha M, *et al.* Endothelial Ca2+ signaling, angiogenesis and vasculogenesis: Just what it takes to make a blood vessel. Int J Mol Sci 2019;20(16):3962.
48. Goukassian DA, Qin G, Dolan C, *et al.* Tumor necrosis factor-α receptor p75 is required in ischemia-induced neovascularization. Circulation 2007;115(6):752-762.
49. Tsatralis T, Ridiandries A, Robertson S, *et al.* Reconstituted high-density lipoproteins promote wound repair and blood flow recovery in response to ischemia in aged mice. Lipids Health Dis 2016;15(1):150.
50. Arcondéguy T, Lacazette E, Millevoi S, *et al.* VEGF-A mRNA processing, stability and translation: A paradigm for intricate regulation of gene expression at the post-transcriptional level. Nucleic Acids Res 2013;41(17):7997-8010.
51. Musumeci G, Castorina A, Magro G, *et al.* Enhanced expression of CD31/platelet endothelial cell adhesion molecule 1 (PECAM1) correlates with hypoxia inducible factor-1 alpha (HIF-1α) in human glioblastoma multiforme. Exp Cell Res 2015;339(2):407-416.
52. Jin ML, Zou ZH, Tao T, *et al.* Effect of the recombinant adenovirus-mediated HIF-1 alpha on the expression of VEGF in the hypoxic brain microvascular endothelial cells of rats. Neuropsychiatr Dis Treat 2020;16:397-406.
53. Mor F, Quintana FJ, Cohen IR. Angiogenesis-inflammation cross-talk: Vascular endothelial growth factor is secreted by activated T cells and induces Th1 polarization. J Immunol 2004;172(7):4618-4623.